

To appear in The Astrophysical Journal

High Angular Resolution Observations of the Collimated Jet Source Associated with a Massive Protostar in IRAS 16547-4247

Luis F. Rodríguez

*Centro de Radioastronomía y Astrofísica, UNAM, Apdo. Postal 3-72, Morelia, Michoacán,
58089 México*

`l.rodriguez@astrosmo.unam.mx`

Guido Garay

Departamento de Astronomía, Universidad de Chile, Casilla 36-D, Santiago, Chile

`guido@das.uchile.cl`

Kate J. Brooks

Australia Telescope National Facility, P.O. Box 76, Epping NSW 1710 Australia

`Kate.Brooks@atnf.csiro.au`

and

Diego Mardones

Departamento de Astronomía, Universidad de Chile, Casilla 36-D, Santiago, Chile

`mardones@das.uchile.cl`

ABSTRACT

A triple radio source recently detected in association with the luminous infrared source IRAS 16547-4247 has been studied with high angular resolution and high sensitivity with the Very Large Array at 3.6 and 2 cm. Our observations confirm the interpretation that the central object is a thermal radio jet, while the two outer lobes are most probably heavily obscured HH objects. The thermal radio jet is resolved angularly for the first time and found to align closely with the outer lobes. The opening angle of the thermal jet is estimated to be $\sim 25^\circ$,

confirming that collimated outflows can also be present in massive protostars. The proper motions of the outer lobes should be measurable over timescales of a few years. Several fainter sources detected in the region are most probably associated with other stars in a young cluster.

Subject headings: ISM: individual (IRAS 16547-4247) — ISM: jets and outflows — radio continuum: stars — stars: formation

1. Introduction

Perhaps the major question related with galactic star formation is whether or not the successful model of low-mass star formation, based on accretion via a circumstellar disk and collimated outflow in the form of jets (Shu, Adams, & Lizano 1987), can be extended to the case of high-mass protostars. A handful of B-type young stars have been found to be associated with collimated outflows and even possibly circumstellar disks (see Garay & Lizano 1999). The source studied here, IRAS 16547-4247, is possibly the best case of a highly collimated outflow associated with an O-type protostar.

IRAS 16547-4247 is a region of star formation located at a distance of 2.9 kpc. It has a bolometric luminosity of $6.2 \times 10^4 L_{\odot}$, equivalent to that of a single O8 zero-age main-sequence star, although most probably a cluster is present and the most massive star is of slightly lower luminosity. Garay et al. (2003) recently detected an embedded triple radio continuum source associated with the IRAS source. The three radio components are aligned in a northwest-southeast direction, with the outer lobes symmetrically separated from the central source by an angular distance of $\sim 10''$, equivalent to a physical separation in the plane of the sky of ~ 0.14 pc. The positive spectral index of the central source is consistent with that expected for a radio thermal (free-free) jet (e. g. Anglada 1996; Rodríguez 1997), while the spectral index of the lobes suggests non thermal emission. The triple system is centered on the position of the IRAS source and is also coincident within error with a 1.2 mm dust continuum and molecular line emission core whose mass is of order $10^3 M_{\odot}$ (Garay et al. 2003). Brooks et al. (2003) reported a chain of H_2 2.12 μm emission knots that trace a collimated flow extending over 1.5 pc that emanates from close to the central component of the triple radio source and has a position angle very similar to that defined by the outer lobes of the triple radio source. Most likely this extended component traces gas ejected in the past by the central component of the triple source.

In this paper we present sensitive, high angular resolution Very Large Array observations and new ATCA radio continuum observations that provide new information on the

characteristics of the radio triple source in IRAS 16547-4247.

2. Observations

The observations were made using the Very Large Array (VLA) of the National Radio Astronomy Observatory (NRAO)¹ and the Australia Telescope Compact Array (ATCA)² in Australia.

2.1. Very Large Array

The VLA radio continuum observations were carried out in 2003 September 25 and 30, at the frequencies of 8.46 and 14.9 GHz. The array was in the BnA configuration and an effective bandwidth of 100 MHz with two circular polarizations was employed. The absolute amplitude calibrator was 1331+305 (with adopted flux densities of 5.21 and 3.46 Jy, at 8.46 and 14.9 GHz, respectively). At 14.9 GHz the 1331+305 data were used in conjunction with a source model provided by NRAO. The phase calibrator was 1626–298, with the bootstrapped flux densities given in Table 1. The phase center of the array was $\alpha = 16^h58^m17^s.202$ and $\delta = -42^\circ52'09''.59$ (J2000.0). The data were edited and calibrated using the software package Astronomical Image Processing System (AIPS) of NRAO. To correct for amplitude and phase noise induced by the low elevation of the source, the data were self-calibrated. No significant variations were found between the two epochs of observations (separated by only five days) and the final analysis was made concatenating all data. Cleaned maps were obtained using the task IMAGR of AIPS. The synthesized (FWHM) beams are $1.13'' \times 0.61''$ and $0.95'' \times 0.42''$ at the frequencies of 8.46 and 14.9 GHz, respectively. The noise level achieved in the images are 30 and 87 $\mu\text{Jy beam}^{-1}$ at 8.46 and 14.9 GHz, respectively.

2.2. ATCA

The ATCA radio continuum observations were made in 2003, February 28, using the 6A configuration, which utilizes all six antennas and covers east-west baselines from 300 m to 5.9

¹NRAO is a facility of the National Science Foundation operated under cooperative agreement by Associated Universities, Inc.

²The Australia Telescope Compact Array is funded by the Commonwealth of Australia for operation as a National Facility managed by CSIRO.

km. Observations were made at the frequencies of 4.80 and 8.64 GHz, each with a bandwidth of 128 MHz. The phase center of the array was $\alpha = 16^h58^m16^s847$ and $\delta = -42^\circ51'37''.23$ (J2000.0). The total integration time at each frequency was 285 minutes, obtained from 15-minute scans taken over a range of hour angles to provide good (u,v) plane coverage. The calibrator 1616-52 was observed before and after every on-source scan in order to correct the amplitude and phase of the interferometer data for atmospheric and instrumental effects. The same calibrator was also used for the bandpass correction. The flux density was calibrated by observing PKS 1934-638 (3C84) for which values of 5.83 and 2.84 Jy at 4.8 and 8.6 GHz, respectively, were adopted. Standard calibration and data reduction were performed using MIRIAD (Sault, Teuben, & Wright 1995). Maps were made by Fourier transformation of the uniformly weighted interferometer data using the AIPS task MX. The synthesized (FWHM) beams are $4.08'' \times 1.49''$ and $2.32'' \times 0.80''$ at the frequencies of 4.80 and 8.64 GHz, respectively. The noise level achieved in the images are 70 and 72 $\mu\text{Jy beam}^{-1}$ at 4.80 and 8.64 GHz, respectively.

3. Results and Discussion

Figures 1 and 2 present contour maps of the emission observed, respectively, with ATCA (4.80 and 8.64 GHz) and with the VLA (8.46 and 14.9 GHz). These images show that there are three dominant sources that Garay et al. (2003) identified as the central source and the two (north and south) outer lobes. The high sensitivity and angular resolution of the 8.46 GHz VLA image allowed us to resolve the spatial structure of these features and to detect several other components, which will be discussed in what follows. Table 2 presents the positions, flux densities and deconvolved angular dimensions of the sources associated with the triple radio continuum system (jet and two lobes). The observed parameters were determined from a linearized least-squares fit to a Gaussian ellipsoid function using the task IMFIT of AIPS.

We note that the 8.46 GHz flux densities measured for the three main sources with the VLA in 2003 September are similar (within a factor of 1.2) to the 8.64 GHz flux densities measured with ATCA in 2003 February and larger by factors of 1.5 to 2 with respect to the 8.64 GHz flux densities reported by Garay et al. (2003) from observations taken with ATCA in 2000 May. Although we cannot rule out a calibration problem, we believe that this difference could be due to the well known fact that both thermal jets (Rodríguez et al. 2001; Galván-Madrid, Avila, & Rodríguez 2004) and HH knots (Rodríguez et al. 2000) can show significant flux density variations on scales of years or even months.

3.1. The central source

From the ATCA observations we measured that the central source has flux densities of 7.3 ± 0.4 mJy at 4.8 GHz and 8.2 ± 0.2 mJy at 8.64 GHz. From the VLA observations we measured flux densities of 8.7 ± 0.1 mJy at 8.46 GHz and 10.5 ± 0.3 mJy at 14.9 GHz. Assuming that the flux density has a power law dependence with frequency of the form $S_\nu \propto \nu^\alpha$, we derive that the central source has a spectral index of 0.33 ± 0.05 between 8.46 and 14.9 GHz, similar to the value of 0.49 derived by Garay et al. (2003) and consistent with free-free emission from a collimated jet.

The central source is clearly resolved angularly with the VLA (see Figure 2). We determined deconvolved major and minor axis of $1.02'' \times 0.22''$, P.A. of 163° , at 8.46 GHz, and $0.74'' \times 0.22''$, P.A. 167° , at 14.9 GHz. Assuming that the angular size of the major axis of the central source has a power law dependence with frequency of the form $\theta_\nu \propto \nu^\beta$, we find that this object has a power law angular size index of -0.56 ± 0.05 , consistent with the values expected for a thermal jet source (Reynolds 1986), whose angular dimensions diminish with increasing frequency. We assume that the opening angle of the thermal jet is the angle subtended by the deconvolved minor axis at a distance of one half the deconvolved major axis (Eislöffel et al. 2000), namely that the opening angle is two times the arctan of the ratio of the deconvolved minor axis over the deconvolved major axis. Using the 8.46 GHz deconvolved angular dimensions given in Table 2, we then estimate the opening angle of the thermal jet to be $\sim 25^\circ$, indicating significant collimation in this massive protostar.

3.2. The north lobe

The 8.46 GHz VLA image shows that the north lobe has a string-like structure, that almost connects the north tip of the lobe with the central source. The structure is composed of at least three components, labeled N-1, N-2 and N-3, which are also seen in the 8.64 GHz ATCA map. These three components are along the outflow axis and we will consider them to be knots in the jets. At 14.9 GHz, emission from the north lobe is detected only from the brighter 8.46 GHz knot (component N-1).

Due to the different angular resolution at the different frequencies and the blending of emission from the different components in the northern lobe it is not straightforward to derive the spectral index of their emission. To partially avoid this problem we made tapered maps of the emission at the higher frequencies observed with ATCA and with the VLA. The taper value was chosen to match the beam at the lower frequency. Using the ATCA data we measure at the peak position of the north lobe peak flux densities of 2.67 mJy beam $^{-1}$ at 4.80

GHz (HPBW of $4.08'' \times 1.49''$) and $2.45 \text{ mJy beam}^{-1}$ at 8.64 GHz (HPBW of $4.05'' \times 1.48''$), implying a spectral index of -0.15 ± 0.09 . From the VLA observations, we find that the N-1 component has a spectral index of 0.17 ± 0.39 between 8.46 and 14.9 GHz. These results, indicating a flat spectrum, suggest that the radio continuum emission at the peak position of the northern lobe corresponds to optically thin thermal emission. The spectral index of the integrated emission from the whole northern lobe is -0.32 ± 0.29 .

3.3. The south lobe

The 8.46 GHz VLA image shows that the south lobe is composed of a bright component, labeled S-1, and a weak component, labeled S-2. No emission is detected towards this lobe connecting the bright component with the central source. The triple source in IRAS 16547-4247 is similar to the triple source in Serpens (Curiel et al. 1993), in the sense that both show one side with many knots connecting a lobe with the central source, while there is no detectable emission between the central source and the other lobe.

Using the ATCA data set with similar beams, we determined a spectral index between 4.8 and 8.64 GHz of -0.36 ± 0.09 for the peak flux density and of -0.65 ± 0.14 for the integrated emission from S-1. Using the VLA data, we measure flux densities of $2.8 \pm 0.1 \text{ mJy}$ at 8.46 GHz and $2.0 \pm 0.1 \text{ mJy}$ at 15 GHz, implying a spectral index of -0.59 ± 0.15 . These results suggest that the emission from the southern lobe has a non thermal origin. A detailed discussion on the presence of thermal and non thermal components in this type of objects is given in Garay et al. (1996). The duality in emission mechanisms is expected in shock waves where a small fraction of the electrons are accelerated to relativistic velocities, giving rise to nonthermal emission, while most of the electrons produce thermal free-free emission (Crusius-Wätzel 1990; Henriksen, Ptuskin, & Mirabel 1991). It is interesting to note that the outflows where a non thermal component has been found (Serpens: Rodríguez et al. 1989, HH 80-81: Martí, Rodríguez, & Reipurth 1993, Cep A: Garay et al. 1996, W3(OH): Wilner, Reid, & Menten 1999, IRAS 16547-4247: this paper) are all associated with massive young stellar objects.

3.4. Alignment and proper motions

For each of the three main sources, the position angles of the major axis determined with the VLA at 8.46 and 14.9 GHz are consistent within error. The position angle of the major axis of the central thermal jet is, from the more accurate 8.46 GHz data, $163^\circ \pm 1^\circ$. This

position angle agrees extremely well with the position angle of $163^\circ \pm 1^\circ$ determined from the 8.46 GHz positions given in Table 2 for the N-1 and S-1 components. However, as first noted by Garay et al. (2003), there is a slight misalignment between the lobes and the central source (see Figure 2), in the sense that the central source is displaced by about $0''.5$ to the northeast of the line that joins the lobes. Garay et al. (2003) propose that this displacement could be explained in terms of a jet that is ejected from a source with an orbital motion (Masciadri & Raga 2002). Similar small misalignments have been found in other thermal jet sources: L1551 IRS5 (see Figure 1 of Rodríguez et al. 2003), HH 1-2 (see Figure 1 of Rodríguez et al. 2000), and HH 80-81 (see Figure 1 of Martí, Rodríguez, & Reipurth 1993 and Figures 2 and 3 of Martí, Rodríguez, & Reipurth 1998). Since there are only a handful of triple radio sources where both lobes and the central source are simultaneously detected, this misalignment appears to be rather common among these sources and deserves further investigation.

Given the high signal to noise ratio of the image, the relative positions of the sources can be determined with great accuracy from the images. From the 8.46 GHz image we get an angular separation of $20''.38 \pm 0''.02$ between the N-1 and S-1 components, whereas at 2 cm this angular separation is found to be $20''.40 \pm 0''.11$. Assuming that the knots move at 500 km s^{-1} in the plane of the sky, we expect their separation to increase by $0''.2$ in a three year period and we should be able to determine proper motions at a $10\text{-}\sigma$ accuracy by obtaining a new 8.46 GHz image in 2006. It is very important to measure the proper motions of these knots, since the detection of large values will corroborate the interpretation that a massive protostar is producing the outflow. Jets from massive protostars are characterized by larger velocities ($500\text{-}1000 \text{ km s}^{-1}$; Martí, Rodríguez, & Reipurth 1995) than jets from low mass protostars (where velocities below 300 km s^{-1} are the rule; e. g. Reipurth et al. 2000, Bally et al. 2002).

3.5. Other sources in the field

In the 14.9 GHz VLA image (see Figure 2) we only detect the central source and the brighter components of the lobes (N-1 and S-1) above the $5\text{-}\sigma$ level. The 8.46 GHz VLA image is several times more sensitive and besides the central source and the two outer lobes, three other components, labeled A, B and C, are detected. They are clearly displaced from the main axis of the outflow. Their positions and flux densities are given in Table 3.

Source A, located $\sim 4''$ northeast of N-1, seems to be part of a complex structure associated with the northern lobe. Emission from this source was detected with ATCA at 4.8 and 8.64 GHz, with flux densities of 1.7 ± 0.3 and 1.2 ± 0.4 mJy, respectively. The flux

density measured with the VLA at 8.46 GHz is about a third of that measured with ATCA at 8.64 GHz, suggesting that most of the emission is resolved out with the high angular resolution VLA observations.

Source B was detected with the VLA at 8.46 GHz (September, 2003), with a flux density of 0.67 mJy, but it was below the detection limits at 8.64 GHz when observed with ATCA (February, 2003). Garay et al. (2003) detected source B at 8.64 GHz with a flux density of 0.9 mJy during May, 2000. These observations indicate that source B is time variable. In addition, we detected emission from source B at 4.8 GHz with ATCA with a flux density of 0.44 mJy.

Source C was detected with ATCA at 4.8 and 8.64 GHz, with flux densities of 1.08 ± 0.05 and 0.74 ± 0.06 mJy, respectively. It was clearly detected with the VLA at 8.46 GHz, with a flux density of 0.90 mJy, and marginally detected at 14.9 GHz, with a flux density of 0.64 ± 0.20 mJy. Source C is not present in the 8.64 GHz image of Garay et al. (2003) indicating it is time variable. The spectral index derived from the 4.8 and 8.64 GHz ATCA flux densities is -0.6 ± 0.2 , in good agreement with the less reliable spectral index between 8.46 and 14.9 GHz derived from the VLA data, suggestive of a non thermal spectrum. In addition, source C was found to be unresolved in all the observed frequencies. We propose that this source could be associated with a young, low-mass star with gyrosynchrotron emission (see Gómez, Rodríguez, & Garay 2002).

LFR is grateful to CONACyT, México and DGAPA, UNAM for their support. DM and GG acknowledge support from the Chilean Centro de Astrofísica FONDAF 15010003.

REFERENCES

- Anglada, G. 1996, in ASP Conf. Ser. 93, Radio Emission from the Stars and the Sun, ed. A. R. Taylor & J. M. Paredes (San Francisco: ASP), 3
- Bally, J., Heathcote, S., Reipurth, B., Morse, J., Hartigan, P., & Schwartz, R. 2002, AJ, 123, 2627
- Brooks, K. J., Garay, G., Mardones, D., & Bronfman, L. 2003, ApJ, 594, L131
- Crusius-Wätzell, A. R. 1990, ApJ, 361, L49
- Curiel, S., Rodríguez, L. F., Moran, J. M., & Cantó, J. 1993, ApJ, 415, 191

- Eislöffel, J., Mundt, R., Ray, T. P., & Rodríguez, L. F. 2000, in *Protostars and Planets IV*, ed. V. Mannings, A. P. Boss, & S. S. Russell (Tucson: Univ. Arizona Press), 815
- Galván-Madrid, R., Avila, R., & Rodríguez, L. F. 2004, *RevMexA&A*, 40, 31
- Garay, G., Ramirez, S., Rodríguez, L. F., Curiel, S., & Torrelles, J. M. 1996, *ApJ*, 459, 193
- Garay, G., & Lizano, S. 1999, *PASP*, 111, 1049
- Garay, G., Brooks, K. J., Mardones, D., & Norris, R. P. 2003, *ApJ*, 587, 739
- Gómez, Y., Rodríguez, L. F., & Garay, G. 2002, *ApJ*, 571, 901
- Henriksen, R. N., Ptuskin, V. S., & Mirabel, I. F. 1991, *A&A*, 248, 221
- Martí, J., Rodríguez, L. F., & Reipurth, B. 1993, *ApJ*, 416, 208
- Martí, J., Rodríguez, L. F., & Reipurth, B. 1995, *ApJ*, 449, 184
- Martí, J., Rodríguez, L. F., & Reipurth, B. 1998, *ApJ*, 502, 337
- Masciadri, E., & Raga, A. C. 2002, *ApJ*, 568, 733
- Reipurth, B., Heathcote, S., Morse, J., Hartigan, P., & Bally, J. 2002, 123, 362
- Reynolds, S. P. 1986, *ApJ*, 304, 713
- Rodríguez, L. F., Curiel, S., Moran, J. M., Mirabel, I. F., Roth, M. & Garay, G. 1989, *ApJ*, 346, L85
- Rodríguez, L. F. 1997, in *Herbig-Haro Flows and the Birth of Low Mass Stars*, proceedings of IAU Symp. No. 182, eds. B. Reipurth & C. Bertout, p. 83 (Dordrecht: Kluwer)
- Rodríguez, L. F., Delgado-Arellano, V. G., Gómez, Y., Reipurth, B., Torrelles, J. M., Noriega-Crespo, A., Raga, A. C., & Cantó, J. 2000, *AJ*, 119, 882
- Rodríguez, L. F., Torrelles, J. M., Anglada, G., & Martí, J. 2001, *RevMexA&A*, 37, 95
- Rodríguez, L. F., Porras, A., Claussen M. J., Curiel, S., Wilner, D. J., & Ho, P. T. P. 2003, *ApJ*, 586, L139
- Shu, F. H., Adams, F. C., & Lizano, S. 1987, *ARA&A*, 25, 23
- Wilner, D. J., Reid, M. J., & Menten, K. M. 1999, *ApJ*, 513, 775

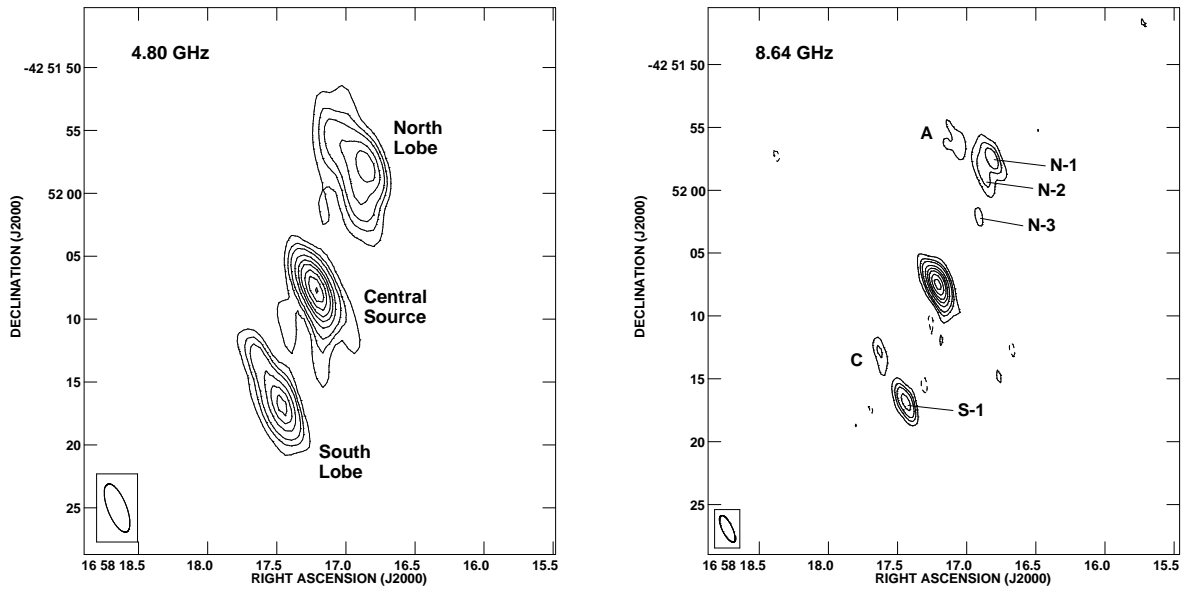


Fig. 1.— ATCA images at 4.80 (left) and 8.64 GHz (right) towards IRAS 16547-4247. Contours are -1, 1, 2, 3, 5, 7, 9, 12, 15, and 18 times $0.3 \text{ mJy beam}^{-1}$. The half power contour of the synthesized beams ($4''.08 \times 1''.49$; $\text{PA} = 22^\circ$ for the 4.8 GHz image and $2''.32 \times 0''.80$; $\text{PA} = 26^\circ$ for the 8.6 GHz image) are shown in the bottom left corner of each panel.

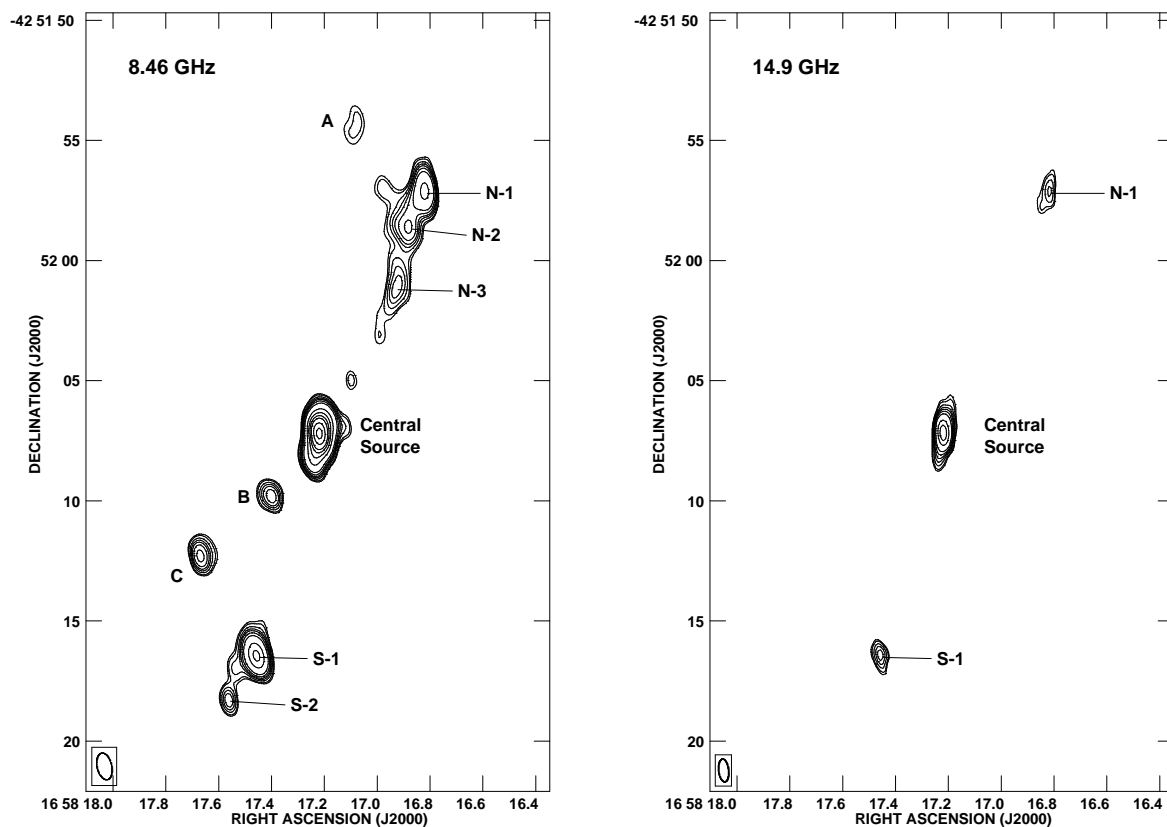


Fig. 2.— VLA images at 8.46 (left) and 14.9 GHz (right) towards IRAS 16547-4247. Contours are $-5, 5, 6, 8, 10, 12, 15, 20, 40, 60, 80, 100, 140,$ and 180 times 30 and $87 \mu\text{Jy beam}^{-1}$, the rms of the 8.46 and 14.9 GHz images, respectively. The half power contour of the synthesized beams ($1''.13 \times 0''.61$; $\text{PA} = 13^\circ$ for the 8.46 GHz image and $0''.95 \times 0''.42$; $\text{PA} = 6^\circ$ for the 14.9 GHz image) are shown in the bottom left corner of each panel. The 8.46 GHz image was made with a ROBUST=0 weighting, while the 14.9 GHz image was made with a ROBUST=5 weighting.

Table 1. Bootstrapped Flux Densities of the Phase Calibrator (1626-298)

Epoch	Wavelength (cm)	Flux Density (Jy)
2003 September 25	3.6	1.490 ± 0.002
2003 September 30	3.6	1.527 ± 0.003
2003 September 25	2.0	1.819 ± 0.005
2003 September 30	2.0	1.856 ± 0.006

Table 2. Observed parameters of main sources

Comp.	$\alpha(2000)^a$ ($16^h 58^m$)	$\delta(2000)^a$ (-42°)	Frequency (GHz)	S_ν^b (mJy)	Deconvolved Size ^c
Central source					
	$17^s 216 \pm 0.006$	$52' 07'' 64 \pm 0'' 05$	4.80	7.3 ± 0.4	$2'' 0 \pm 0'' 2 \times 1'' 1 \pm 0'' 1$; $24^\circ \pm 10^\circ$
	$17^s 210 \pm 0.003$	$52' 07'' 48 \pm 0'' 02$	8.64	8.2 ± 0.2	$1'' 39 \pm 0'' 06 \times 0'' 80 \pm 0'' 04$; $9^\circ \pm 4^\circ$
	$17^s 218 \pm 0.001$	$52' 07'' 22 \pm 0'' 01$	8.46	8.7 ± 0.1	$1'' 02 \pm 0'' 01 \times 0'' 22 \pm 0'' 02$; $163^\circ \pm 1^\circ$
	$17^s 219 \pm 0.001$	$52' 07'' 16 \pm 0'' 01$	14.9	10.5 ± 0.3	$0'' 74 \pm 0'' 02 \times 0'' 22 \pm 0'' 03$; $167^\circ \pm 2^\circ$
North lobe					
N-1...	$16^s 815 \pm 0.009$	$51' 57'' 44 \pm 0'' 07$	8.64	1.8 ± 0.2	$1'' 29 \pm 0'' 18 \times 0'' 53 \pm 0'' 07$; $28^\circ \pm 10^\circ$
	$16^s 821 \pm 0.001$	$51' 57'' 08 \pm 0'' 01$	8.46	2.0 ± 0.1	$1'' 30 \pm 0'' 03 \times 0'' 37 \pm 0'' 05$; $159^\circ \pm 2^\circ$
	$16^s 824 \pm 0.005$	$51' 57'' 17 \pm 0'' 06$	14.9	2.2 ± 0.4	$1'' 59 \pm 0'' 11 \times 0'' 41 \pm 0'' 06$; $168^\circ \pm 3^\circ$
N-2...	$16^s 883 \pm 0.01$	$51' 58'' 63 \pm 0'' 1$	8.64	1.6 ± 0.3	$2'' 74 \pm 0'' 25 \times 0'' 60 \pm 0'' 13$; $17^\circ \pm 4^\circ$
	$16^s 893 \pm 0.004$	$51' 58'' 39 \pm 0'' 03$	8.46	1.5 ± 0.2	$1'' 81 \pm 0'' 06 \times 0'' 97 \pm 0'' 03$; $180^\circ \pm 3^\circ$
N-3...	$16^s 912 \pm 0.01$	$52' 02'' 13 \pm 0'' 1$	8.64	0.4 ± 0.1^d	—
	$16^s 931 \pm 0.004$	$52' 01'' 16 \pm 0'' 03$	8.46	1.0 ± 0.1	$1'' 76 \pm 0'' 06 \times 0'' 54 \pm 0'' 05$; $165^\circ \pm 2^\circ$
South lobe					
S-1...	$17^s 462 \pm 0.007$	$52' 16'' 91 \pm 0'' 06$	4.80	4.1 ± 0.2	$1'' 92 \pm 0'' 22 \times 1'' 19 \pm 0'' 14$; $6^\circ \pm 12^\circ$
	$17^s 441 \pm 0.004$	$52' 16'' 83 \pm 0'' 03$	8.64	2.8 ± 0.1	$0'' 91 \pm 0'' 16 \times 0'' 31 \pm 0'' 32$; $175^\circ \pm 5^\circ$
	$17^s 459 \pm 0.002$	$52' 16'' 43 \pm 0'' 01$	8.46	2.8 ± 0.1	$0'' 66 \pm 0'' 04 \times 0'' 46 \pm 0'' 02$; $20^\circ \pm 7^\circ$
	$17^s 459 \pm 0.003$	$52' 16'' 45 \pm 0'' 03$	14.9	2.0 ± 0.1	$0'' 66 \pm 0'' 07 \times 0'' 41 \pm 0'' 04$; $15^\circ \pm 11^\circ$
S-2...	$17^s 561 \pm 0.003$	$52' 18'' 26 \pm 0'' 03$	8.46	0.42 ± 0.05	— ^e

^aPeak position. Right ascension (α) given in hours, minutes, and seconds, and declination (δ), given in degrees, arcmin, and arcsec. The errors given are formal statistical errors. The absolute positional error of the images is estimated to be $0''.2$.

^bTotal flux density.

^cDeconvolved dimensions of the source: FWHM major axis \times FWHM minor axis; position angle of major axis.

^dPeak flux density (mJy beam⁻¹).

^eUnresolved

Table 3. Parameters of the sources away from the outflow axis

Source	$\alpha(2000)^a$ ($16^h 58^m$)	$\delta(2000)^a$ (-42°)	Frequency (GHz)	S_ν^b (mJy)
A....	$17^s162\pm0.027$	$51' 56''87\pm1''04$	4.80	1.7 ± 0.3
	$17^s069\pm0.025$	$51' 56''11\pm0''18$	8.64	1.2 ± 0.4
	$17^s084\pm0.005$	$51' 54''55\pm0''13$	8.46	0.38 ± 0.05
B....	$17^s423\pm0.047$	$52' 10''38\pm0''64$	4.80	0.44 ± 0.05
	$17^s404\pm0.002$	$52' 09''79\pm0''02$	8.46	0.67 ± 0.05
	$17^s407\pm0.01$	$52' 09''68\pm0''09$	14.9	0.70 ± 0.24
C....	$17^s652\pm0.023$	$52' 12''98\pm0''20$	4.80	1.08 ± 0.05
	$17^s623\pm0.010$	$52' 13''08\pm0''11$	8.64	0.74 ± 0.06
	$17^s665\pm0.001$	$52' 12''26\pm0''02$	8.46	0.90 ± 0.06
	$17^s641\pm0.008$	$52' 12''05\pm0''06$	14.9	0.64 ± 0.20

^aPeak position. Right ascension (α) given in hours, minutes, and seconds, and declination (δ), given in degrees, arcmin, and arcsec. The errors given are formal statistical errors. The absolute positional error of the images is estimated to be $0''.2$.

^bTotal flux density.